Journal of Ovonic Research Vol. 20, No. 4, July - August 2024, p. 455 - 466

Effect of post-annealing treatment on structural, optical and photocatalytic properties of TiO_2 nanoparticles prepared via pulsed laser ablation in liquid

Z. Liu [a,b], R. X. Wang[a,*]
[a]*School of Science, Jinling Institute of Technology, Nanjing 210093, China*
[b]*College of Engineering and Applied Sciences, Nanjing University, Nanjing 210093, P. R. China*

Ultrasmall TiO_2 nanoparticles were synthesized through pulsed laser ablation of a metal titanium target in liquid followed by thermal annealing treatment. The impact of post-annealing treatment on the structural, morphological, optical properties, and the photocatalytic activity of the synthesized TiO_2 nanoparticles have been investigated through a variety of analytical techniques, including X-Ray diffraction, transmission electron microscopy, ultraviolet-visible diffusion reflectance spectra, X-ray photoelectron spectroscopy. The results reveal that annealing temperature significantly improved the crystallinity of laser ablated TiO_2 nanoparticles and modified the chemical states of surface elements. Defects introduced by laser ablation, which serve as electron traps, combined with enhanced crystallinity resulting from thermal annealing, have improved the photocatalytic degradation performance of TiO_2 nanoparticles. Specifically, TiO_2 nanoparticles annealed at 300 ℃ exhibited optimal photocatalytic performance in decomposition of model dye under the irradiation from xenon lamp, demonstrating the critical role of annealing in improving photocatalytic properties. This study not only broadens the comprehension of the impact of post-treatment on the characteristics of laser-ablated TiO_2 nanoparticles nanoparticles but also highlights their potential for effective wastewater remediation.

(Received May 2, 2024; Accepted July 8, 2024)

Keywords: Photocatalytic degradation, Annealing temperature, Laser ablation in liquid, TiO_2, Nanoparticles

1. Introduction

Nowadays, humankind faces a problem of organic contamination in water due to the widespread use of water-soluble organic materials in pharmaceutical, chemical and textile industry, which are difficult to eliminate through biodegradation [1-3]. The organic pollutants in aquatic environment are toxic and carcinogenic, which posing a threat to the survival of both aquatic and terrestrial life [4]. The purification of contaminated water has garnered significant interest, with numerous strategies were suggested for remediation of wastewater, including adsorption, electrocatalytic, photocatalytic, and photoelectrocatalytic degradation [5-9].

* Corresponding author: wrx@jit.edu.cn
https://doi.org/10.15251/JOR.2024.204.455

As a sustainable and efficient technology, semiconductor photocatalysis can activate semiconductor materials to produce separated electrons and holes through absorbing irradiated light, which play a crucial role in oxidation-reduction reactions for photocatalytic degradation of pollutants. Several kinds of semiconductors, including TiO_2, ZnO, SnO_2, Bi_2O_3, C_3N_4 and BiOCl have been developed for application in degradation of pollutants through photocatalysis [10-15]. Among these semiconductors, TiO_2 has the advantages of excellent chemical stability, non-toxicity, strong redox potential [16]. However, the traditional TiO_2 powders with large energy gap (3.2 eV) can only be excited by ultraviolet light, accounting for roughly about 5% of sunlight, which limits its application in solar driven photocatalysis. Additionally, the long electron migration distance and high recombination rate of photoinduced electrons and holes for traditional TiO_2 powders are detrimental to their photocatalytic efficiency. Thus, several strategies, including the construction of heterojunctions with other semiconductors, the deposition of noble metal co-catalysts, and the doping of metal or non-metal ions, have been proposed to address the limitations of traditional TiO_2 based photocatalysts [17-22].

Besides the chemical composition, the synthesis method of semiconductors also significantly affects their structural, morphological and optical properties, which are crucial factors determining photocatalytic performance. Semiconductor nanoparticles with favorable photocatalytic properties can be synthesized via various of methods. The general methods include sol-gel, hydrothermal, co-precipitation, spray pyrolysis, electrospinning and laser ablation [23-28]. Compared with other methods, pulsed laser ablation in liquid is simple and rapid method for synthesis of ultrasmall nanoparticles [29]. By laser ablation, the solid target in liquid environment can be partially exfoliated and injected into liquid environment. The instantaneous high temperature and high pressure in micro region provide an extreme environment for growth of defect-rich nanoparticles. The defects in nanophotocatalysts may not only act as electron traps, inhibiting recombination of photoinduced electrons and holes, but also provide active sites for reaction [30,31]. The ultrasmall size is beneficial for reducing the electron transfer distance [32]. Inspired by advantages of laser ablation in liquid, it is necessary to develop TiO_2 nanophotocatalysts via laser ablation in liquid and investigate the effect of post-treatment on photocatalytic performance.

Herein, ultrasmall TiO_2 nanoparticles were produced via laser ablation of metal titanium target in water. The effects of post-annealing treatment on structural, morphological, optical properties were analyzed using XRD, TEM and DRS. Surface chemical bonds and states were analyzed by XPS. The photocatalytic properties of synthesized nanophotocatalysts were characterized by degradation of model dye solution upon light irradiation from a xenon lamp. The results indicate annealing can improve the crystallinity of laser ablated TiO_2 nanoparticles, modify the chemical states of surface elements. The synthesized TiO_2 nanoparticles annealed at 300 ℃ have the best photocatalytic performance.

2. Experimental procedures

2.1. Creation of TiO_2 ultrafine nanopowders

Pulsed laser ablation in liquid technique was used to synthesize pristine defect-rich TiO_2 nanoparticles. The wavelength, band width, power of the pulsed laser were 1064 nm, 100 ns and

50 W, respectively. The solid target for ablation was high pure metal titanium target (99.99%, Diameter: 25.4 mm, Thickness: 6 mm, ZhongNuo Advanced Material (Beijing) Technology Co.,Ltd). The liquid medium used in ablation process was deionized water. Before laser ablating, the metal target was sequentially washed by ultrasonication in acetone, ethanol and deionized water. After cleaning, the metal target was securely attached to the bottom of a glass vessel, which was then filled with sufficient deionized water to completely submerge the solid target. The distance between the surface of liquid medium and the titanium target was 10 mm. For providing enough laser energy density for ablation, the laser beam was focused on the upper surface of metal target through a convex lens with focal length of 261 mm. With the help of galvanometers, the focused laser beam was scanned in circular irradiated area with diameter of 20 mm on the surface of metal target. The blue colloidal solution with TiO_2 nanoparticles were obtained by laser ablation of metal titanium target for 60 min. The pristine TiO_2 nanopowders without post thermal annealing treatment (abbreviated as TW) were obtained by centrifugation at 6000 rpm for 10 min and drying in oven at 100 ℃ for 30 min. The dried powders were then annealed in muffle furnace at different temperature, including 200 ℃ , 300 ℃ , 400 ℃ (abbreviated as T200, T300, T400) for investigating the effect of annealing temperature on physicochemical properties of laser ablated TiO_2 nanopowders.

2.2. Characterization of laser ablated TiO_2 nanoparticles

X-ray diffraction (XRD) technique (operating on Bruker D8 Advance, Cu-Kα radiation, λ=0.154 nm, operating at 40 kV, 15 mA, 2θ=20-90°) was utilized to explore the structural information of the laser ablated powders with different annealing temperatures. Transmission electron microscopy (TEM) was employed to examine the size and morphological properties of the acquired TiO_2 nanopowders. X-ray photoelectron spectroscopy (XPS) analysis was performed with a Thermo Scientific K-Alpha instrument to study the elemental components and chemical valence present on the surface of synthesized TiO_2 nanopowders. The obtained titanium dioxide (TiO_2) nanopowders underwent diffusion reflectance spectra (DRS) analysis. This analysis was carried out using a spectrophotometer (Shimadzu UV-3600i Plus), which was equipped with a Xenon lamp and integrating sphere. $BaSO_4$ powders were served as background material for DRS measurements. The photocatalytic properties the laser ablated TiO_2 nanopowders were evaluated by the degradation of dye in pollutant solutions. RhB was used as the target dye pollutant. Photocatalytic degradation experiments are carried out in a glass vessel filled with 100 ml RhB (10 mg/L) aqueous solutions and 0.05 g synthesized powder catalysts. Before exposure to irradiation, the mixtures were magnetically stirred in dark for 30 min to ensure the adsorption-desorption equilibrium. The xenon lamp (250W) was used as light source for driving photocatalytic reaction. The distance between pollutant solutions and xenon lmap was fixed at 10 cm. During the photocatalytic degradation, 1ml dye solutions were extracted from reactor every 60 min. The extracted mixtures were centrifuged with a centrifugal machine, working at a speed of 6000 rpm, for separating the catalysts and dye solution. The absorption spectra of separated dye solution were recorded with a spectrophotometer (754PC, Shanghai Jinghua) in wavelength range from 300 nm to 700 nm.

3. Results and discussion

Figure 1 displays the XRD patterns of laser ablated TiO_2 nanopowders subjected to varying annealing temperatures, aiming to explore the impact of temperature on crystal structure. As shown, the laser ablated TiO_2 nanopowders without annealing treatment and annealed at 200 ℃ exhibit weak and broad diffraction bands, indicating their amorphous structure. As thermal annealing temperature increase to 300 ℃, the obvious broad diffraction peaks were observed at 25.4°, 27.6°, 36.2°, 41.5°, 54.7°, respectively. It illustrates annealing temperature possesses significant impact on crystallinity of laser ablated TiO_2 nanoparticles. The diffraction peak at 25.4° can be indexed to (101) plane of anatase phase TiO_2, which is consistent with the JCPDS Card No. 21-1272. The diffraction peaks at 27.6°, 36.2°, 41.5°, 54.7° are corresponded to (110), (101), (111), (211) planes of rutile phase TiO_2, which is consistent with JCPDS Card No. 21-1276. With further increase in annealing temperature to 400 ℃, the intensity ratio of anatase phase (101) and rutile phase (110) peaks is obviously changed, indicating the increment of annealing temperature induced phase transition from anatase to rutile phase. In addition, the crystallite size can be calculated from Scherrer formula as the following equation (1).

$$D = \frac{K\lambda}{\beta cos\theta} \tag{1}$$

In the equation, D symbolizes the average grain size, K is shape factor with the value of 0.89, λ signifies the wavelength of the incident X-Ray radiation,which is 0.1542 nm, β represents the full width at half maximum, while θ is the angular position of the diffraction peak. Based on the (101) and (110) peaks of nanopowders annealed at 400 ℃, the grain sizes were determined to be 9 nm for the anatase phase and 5 nm for the rutile phase, respectively. These results demonstrate the ultrasmall nature of the nanoparticles synthesized through the process of laser ablation in liquid [33].

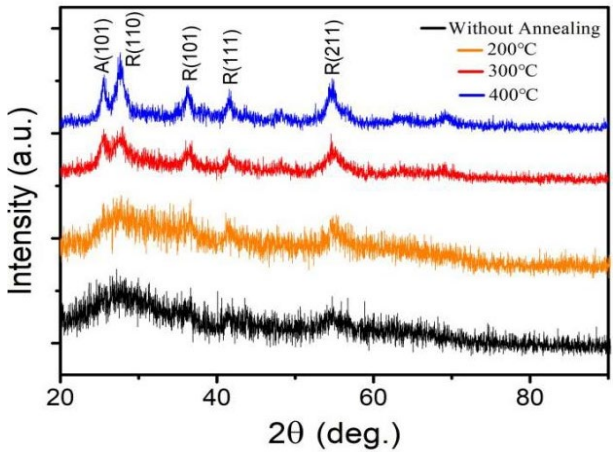

Fig. 1. X-Ray diffractograms of laser ablated TiO_2 nanoparticles annealed at different temperatures.

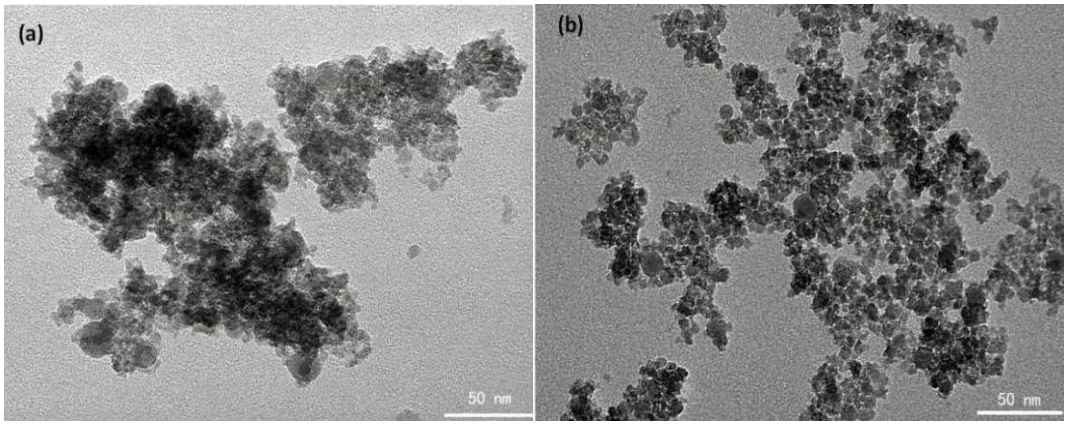

Fig. 2. TEM images of laser ablated TiO_2 nanoparticles, (a) TW, (b)T300.

Fig. 2 (a, b) depict the TEM images of laser ablated TiO_2 nanoparticles, respectively. The TEM micrographs clearly demonstrate that the nanoparticles exhibit a nearly spherical geometry. The sizes of laser ablated nanoparticles are mainly in range from 5 nm to 15 nm for both TW and T300 samples, indicating thermal annealing temperature had little effects on size and morphology of laser ablated TiO_2 nanoparticles.

The chemical bonds and oxidation states of elements on surface of laser ablated TiO_2 photocatalysts were investigated by XPS analysis. Fig. 3 (a, b) display the fine spectra of Ti 2p and O 1s for TW, respectively. Fig. 3 (c, d) present the fine spectra of Ti 2p and O 1s for T300, respectively. As shown in Fig.3 (a, c), the Ti 2p spectra of both TW and T300 can be deconvoluted to four peaks, including 464.4 eV, 458.4 eV for Ti^{4+} and 463.5 eV, 457.9 eV for Ti^{3+}. This result is due to the fact that laser ablation detaches the oxygen atoms from TiO_2 lattice, which favors the reduction of Ti^{4+} to Ti^{3+} by accepting electrons. Compared with TW, the T300 exhibits lower proportion of Ti^{3+}. The possible reason is that Ti^{3+} ions are oxidized by thermal annealing. In Fig. 3 (b), it is observable that O 1s spectra for TW contain three peaks corresponded with different oxygen bonds. The peak at 529.6 eV is associated with lattice O of Ti-O-Ti. The other two peaks, observed at 530.7 eV and 533.1 eV, are associated with oxygen vacancies (V_O) and Ti-OH, respectively. However, only two peaks are observed in O 1s spectra in Fig. 3 (d), which are 529.6 eV for Ti-O-Ti and 530.7 eV for V_O. Meanwhile, by calculating the area of peaks, it can be found that the ratio of V_O to Ti-O-Ti for T300 is lower than TW. The reason for this result is that thermal annealing reduces the number of oxygen vacancies.

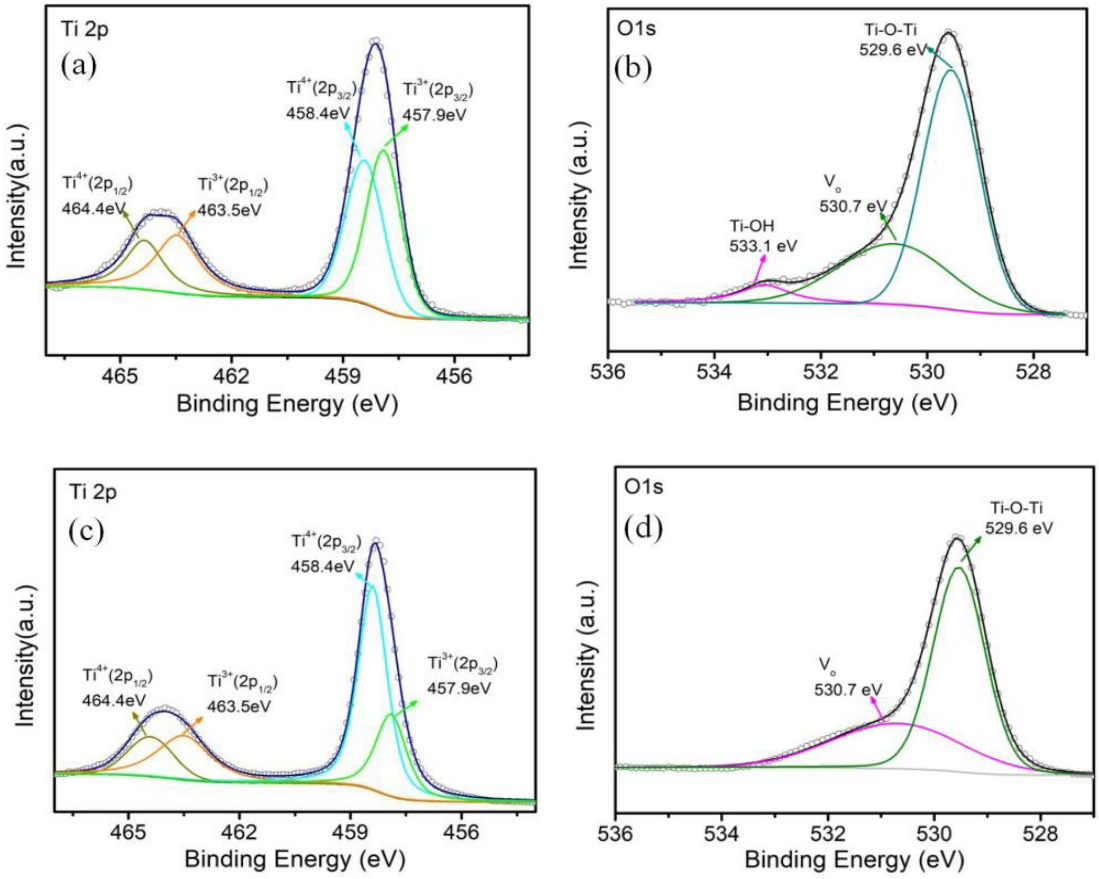

Fig. 3. XPS fine spectra of laser ablated TiO_2, (a) Ti 2p of TW, (b) O 1s of TW, (c)Ti 2p of T300, (d) O1s of T300.

The optical properties of laser ablated TiO_2 nanoparticles, including TW, T200, T300, T400, were explored using UV-Vis DRS. As shown in Fig. 4, the TW has the lowest reflectance in visible range compared with T200, T300 and T400. The annealing temperature exhibits significant influence on reflectance. As the increment of thermal annealing temperature, the reflectance in visible range increase significantly, which is detrimental to improve absorption of visible light wavelengths. By using the Kubelka-Munk function, as detailed in the following equation (2), the reflectance can be converted to absorption coefficients $F(R)$.

$$F(R) = \frac{(1-R)^2}{2R} \tag{2}$$

R represents the reflectance of laser ablated TiO_2 nanoparticles. Fig. 5 shows the $F(R)$ as a function of wavelength. As shown, obvious tails in visible range were observed, indicating presence of the laser ablation induced defect states, which can broaden the absorption range [30]. In addition, the thermal annealing processing has reduced the absorption of laser ablated TiO_2 nanoparticles in the visible wavelength range, suggesting a decrease in number of defects induced by thermal treatment.

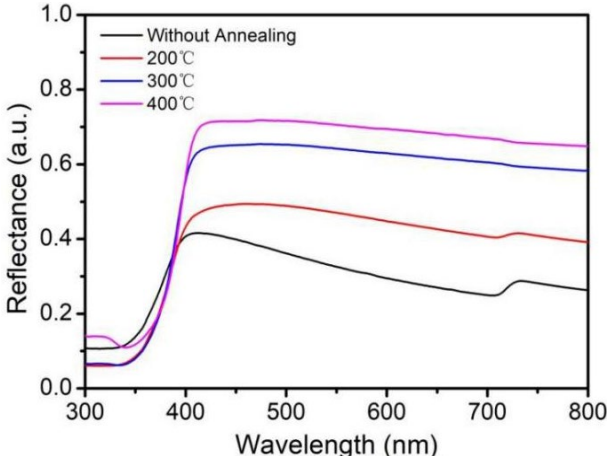

Fig. 4. UV-Vis Diffusion reflectance spectra (DRS) of TW, T200, T300, T400.

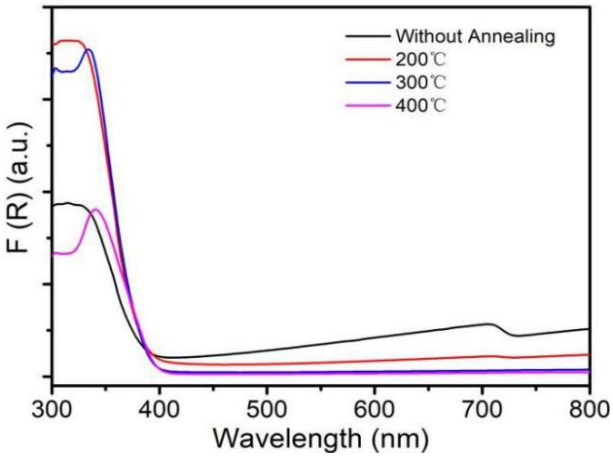

Fig. 5. UV-Vis absorption of TW, T200, T300, T400.

The Tauc plot method can be used to derive the optical band gaps of laser ablated TiO_2 nanoparticles according to the following equation (3),

$$[F(R)hv]^n = \mathrm{A}(hv - E_g) \tag{3}$$

where, h is Plank constant, while v denotes frequency of photon, A is a constant, and E_g represents the bandgap energy of semiconductor. The index n is Tauc exponent, which is determined by the type of transition, which is equal to 2 for direct transition, 1/2 for indirect transition. Fig. 6 presents the Tauc plot of $[F(R)hv]^{1/2}$ versus hv. The energy gap can be obtained from the extrapolating the linear part of the experimental data in Fig. 6. From the intersect point with hv axis, the energy gaps of TW, T200, T300 and T400 are 2.98 eV, 3.04eV, 3.04 eV and 3.03 eV, respectively. Thus, it can be inferred that the annealing temperature slightly changed optical energy gaps of laser ablated TiO_2 nanoparticles. Although the synthesized TiO_2 nanoparticles can absorb visible light, the energy gaps of obtained TiO_2 nanoparticles is close to the ultraviolet region, indicating the laser ablation induced defects played important role in enhancing visible

light absorption. These defect introduced energy states are situated between conduction band and valence band.

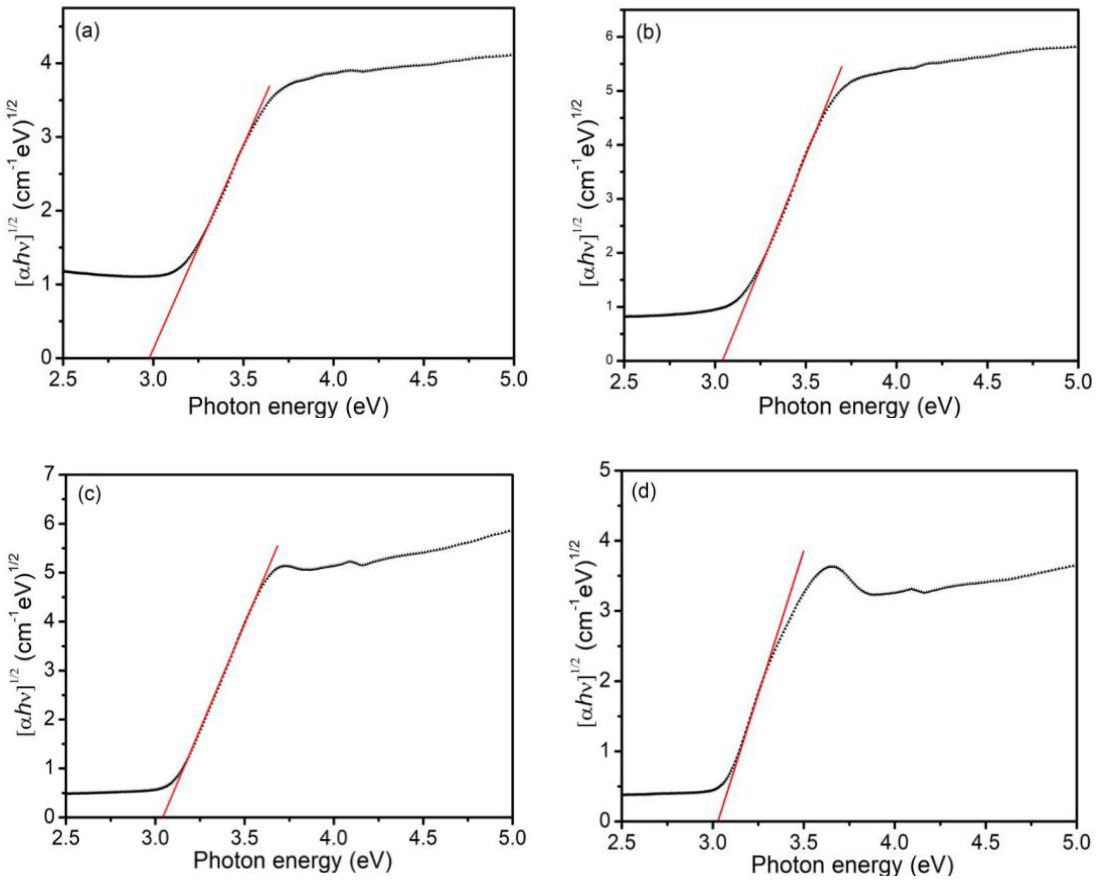

Fig. 6. Tauc Plots of $[F(R)hv]^{1/2}$ *versus hv, (a) TW, (b) T200, (c) T300, (d) T400.*

The photocatalytic activity of semiconductors can be assessed by decomposition of target organic dyes. For investigating the photocatalytic properties, the degradation of RhB dyes over the synthesized TiO_2 nanoparticles upon xenon lamp irradiation were measured. Fig. 7 shows the absorption spectra of extracted dye solution at fixed irradiation time intervals. It is clearly observable that the intensity of absorption band decreases significantly with extended exposure to irradiation. The results indicate the laser ablated TiO_2 nanoparticles are potential nanophotocatalysts for photocatalytic degradation of dye solutions.

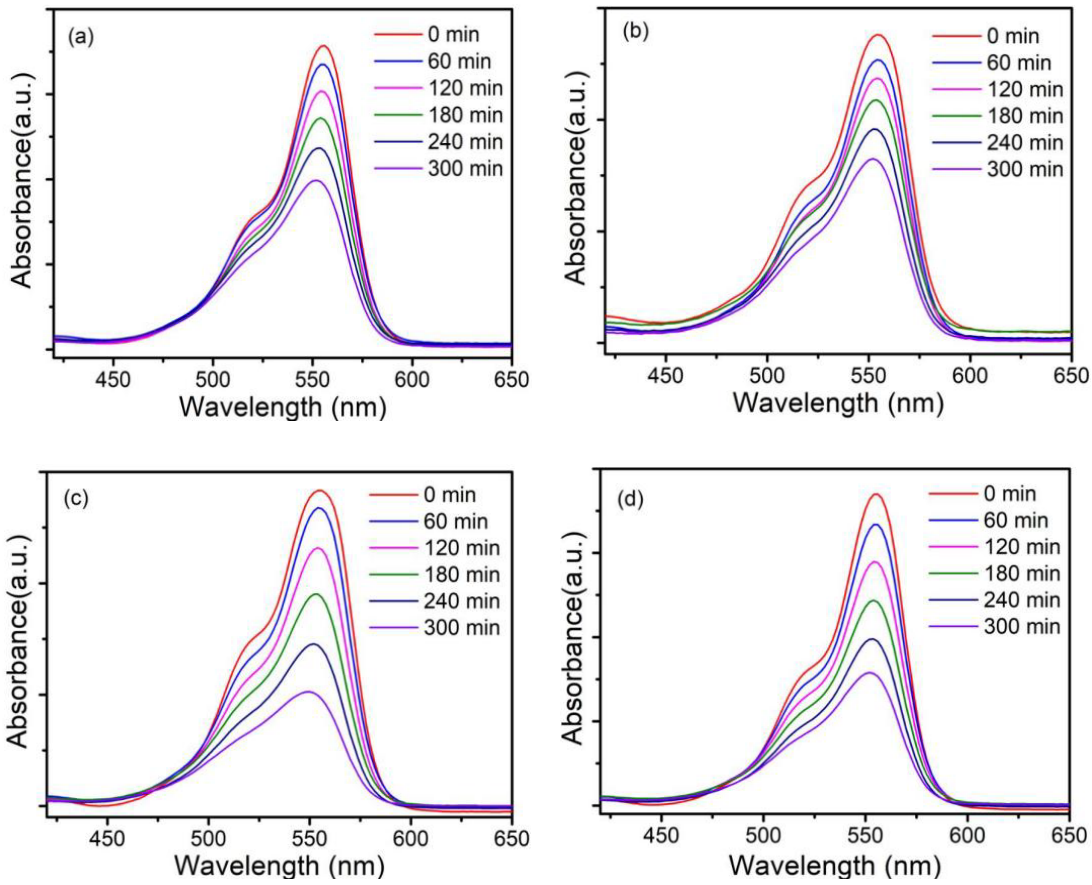

Fig. 7. Absorption spectra of RhB dye solutions over varied photocatalysts at consistent time intervals, (a) TW (b) T200, (c) T300, (d) T400.

The intensities at 554 nm in absorption spectra were recorded to evaluate the concentration of dyes in solutions during the degradation process. The normalized concentration (C/C_0) can be described by normalized absorbance (A/A_0). Furthermore, the photodegradation efficiency (ŋ) can be calculated by the follwing equation (4),

$$\eta = \frac{C_0 - C_t}{C_0} = \frac{A_0 - A_t}{A_0} = 1 - \frac{A_t}{A_0} \quad (4)$$

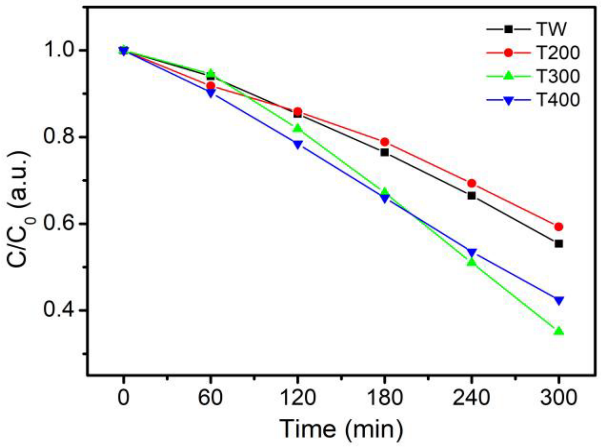

Fig. 8. Normalized concentration of RhB dye in solution during photocatalytic process for TW, T200, T300 and T400.

The concentration of RhB dye as a function of irradiation time was shown in Fig. 8. Following the duration of 300 min, the photocatalytic degradation efficiencies of laser ablated TiO_2 nanophotocatalysts are 44.6%, 40.7%, 64.9% and 57.6% for TW，T200, T300 and T400, respectively. It is demonstrated that the optimal annealing temperature is 300 ℃ for improving the photocatalytic properties of laser ablated TiO_2 nanoparticles.

4. Conclusion

In conclusion, this work has focused on the effect of annealing temperature on structural, morphological, surface chemical, optical and photocatalytic properties of laser ablated TiO_2 nanoparticles. When the annealing temperature is below 200 ℃, the TiO_2 nanoparticles are amorphous. The amorphous TiO_2 can be transformed into crystalline mixed rutile and anatase phase TiO_2 by elevating annealing temperature. XPS analysis demonstrates that laser ablation endows TiO_2 with more defects, which can be reduced via thermal annealing. The annealing temperature slightly modulate the bandgap energy of synthesized nanoparticles. The laser ablated TiO_2 nanoparticles have optimum annealing temperature of 300 ℃ for photocatalytic degradationof RhB dye.

Acknowledgements

This work is funded by Research Start-up Program of Jinling Institute of Technology (jit-b-202054), Natural Science Foundation of Jiangsu Province (BK20201111), Jiangsu Province's Double Innovation Plan (JSSCBS20210616), National Natural Science Foundation of China (Grant No.11804150)

References

[1] Y. L. Chen, F. F. Zhang, S. Y. Guan, W. Shi, X. Y. Wang, C. T. Huang, Q. Chen, Materials Science in Semiconductor Processing 140, 106385 (2022); https://doi.org/10.1016/j.mssp.2021.106385

[2] J. Ebrahimian, M. Mohsennia, M. Khayatkashani, Materials Letters 263, 127255 (2020); https://doi.org/10.1016/j.matlet.2019.127255

[3] Y. Zhang, J. F. Chen, Y. N. Wang, H. C. Dou, Z. P. Lin , X. Gao, X. Q. Chen, M. H. Guo, Applied Surface Science 647, 158985 (2024); https://doi.org/10.1016/j.apsusc.2023.158985

[4] S. Kader, M. R. Al-Mamun, M. B. K. Suhan et al. Environmental Technology & Innovation 27, 102476 (2022); https://doi.org/10.1016/j.eti.2022.102476

[5] L. Sellaoui, M. Bouzidi, D. S.P. Franco, A. S. Alshammari, M. Gandouzi, J. Georgin, N. B. H. Mohamed, A. Erto, M. Badawi , Chemical Engineering Journal 456, 141033 (2023); https://doi.org/10.1016/j.cej.2022.141033

[6] Z. P. Sun, Y. Ni, Y. D. Wu, W. Q. Yue, G. Zhang, J. M. Bai,. Environmental Science and Pollution Research 30, 6262 (2023); https://doi.org/10.1007/s11356-022-22610-y

[7] P. F. Zhou, Y. B. Shen, S. K. Zhao, G. D. Li, B. Y. Cui, D. Z. Wei, Y. S. Shen, Chemical Engineering Journal 407, 126697 (2021); https://doi.org/10.1016/j.cej.2020.126697

[8] S. Fu, Y. Q. Du, J. H. Bie, Z. Q. Huang, H. Hu, Q. Huang, H. J. Zhu, W. Yuan, L. C. Li, Bo Liu, Journal of Science: Advanced Materials and Devices 8, 100561 (2023); https://doi.org/10.1016/j.jsamd.2023.100561

[9] D. H. Yoon, Md R. Ud D. Biswas, A. Sakthisabarimoorthi, Diamond & Related Materials 129, 109363 (2022); https://doi.org/10.1016/j.diamond.2022.109363

[10] K. Pham, H. Ali-Loytty, Jesse Saari, Muhammad Zubair, Mika Valden , Kimmo Lahtonen, Niko Kinnunen, Marianne Gunell, J. J. Saarinen, Optical Materials 131, 112695 (2022); https://doi.org/10.1016/j.optmat.2022.112695

[11] Nurfina Yudasari, Rahma Anugrahwidya, Dahlang Tahir, Maria M. Suliyanti, Yuliati Herbani, Cuk Imawan, Munawar Khalil, Dede Djuhana, Journal of Alloys and Compounds 886, 161291 (2021); https://doi.org/10.1016/j.jallcom.2021.161291

[12] S. X. Hou, S. B. Wu, J. J. Luo, H. E. Ali, S. Eli, Vacuum 212, (2023) 112023; https://doi.org/10.1016/j.vacuum.2023.112023

[13] C. Xu, Q. Zhou, W. Y. Huang, K. Yang, Y. C. Zhang, T. X. Liang, Z. Q. Liu, Rare Metals 41, 2094 (2022); https://doi.org/10.1007/s12598-021-01897-9

[14] J. C. Zhou, B. Gao, D. F. Wu, C. Q. Tian, H. M. Ran, W. Chen, Q. Huang, W. X. Zhang, F. Qi, N. Zhang, Y. Y. Pu, J. Qiu, Z. P. Hu, J. Du, Z. Z. Liu, Y. X. Leng, X. S. Tang, Advanced Functional Materials 34, 2308411 (2024);

[15] C. Y. Chen, T. Jiang, J. H. Hou, T. T. Zhang, G. S. Zhang,Y. C. Zhang, X. Z. Wang Journal of Materials Science and Technology 114, 240 (2022); https://doi.org/10.1016/j.jmst.2021.12.006

[16] A. Raza, H.L. Shen, A. A. Haidry, M. K. Shahzad, R. Liu, S. S. Cui, Applied Surface Science 505, 144540 (2020); https://doi.org/10.1016/j.apsusc.2019.144540

[17] H. F. Yin, Y. Cao, T. L. Fan, B. Qiu, M. Zhang, J. C. Yao, P. F. Li , X. H. Liu, S. M. Chen, Journal of Alloys and Compounds 824, 153915 (2020);

https://doi.org/10.1016/j.jallcom.2020.153915

[18] B. Yu, F. M. Meng, M. W. Khan, Rui Qin, X. B. Liu, Ceramics International 46, 13133 (2020); https://doi.org/10.1016/j.ceramint.2020.02.087

[19] J. Q. Li, Z. W. Zhou, X. Li, Y. L. Yang, J. F. Gao, R. Yu, H. P. Wang, N. Wang, Chemical Engineering Journal 428, 132613 (2022); https://doi.org/10.1016/j.cej.2021.132613

[20] T. Y. Ren, C. M. Feng, J. Dong, H. Zhu, B. Wang, Scientific Reports 12, 10585 (2022); https://doi.org/10.1038/s41598-022-14814-6

[21] P. Pascariu, C. Cojocaru, M. Homocianu, P. Samoila, Journal of Environmental Management 316, 115317 (2022); https://doi.org/10.1016/j.jenvman.2022.115317

[22] H. Liyanaarachchi, C. Thambiliyagodage, C. Liyanaarachchi, U. Samarakoon , Arabian Journal of Chemistry 16, 104749 (2023); https://doi.org/10.1016/j.arabjc.2023.104749

[23] J. Z. Li, J. B. Zhong,J. Zeng, F.M. Feng, J.J. He, Materials Science in Semiconductor Processing 16, 379-384 (2013); https://doi.org/10.1016/j.mssp.2012.09.007

[24] P. Demircivi, B. Gulen, E. B. Simsek, D. Berek 241, 122236 (2020); https://doi.org/10.1016/j.matchemphys.2019.122236

[25] A. I. Meky, M. A. Hassaan, H. A. Fetouh, A. M. Ismail1, A. E. Nemr, Scientifc Reports 13, 19329 (2023); https://doi.org/10.1038/s41598-023-46464-7

[26] S. Karakaya1, L. Kaba1, Journal of Materials Science: Materials in Electronics 34, 1295 (2023);

[27] Petronela Pascariu, Corneliu Cojocaru, Mihaela Homocianu, Petrisor Samoila , Andrei Dascalu, Mirela Suchea, Ceramics International 48, 4953-4964 (2022); https://doi.org/10.1016/j.ceramint.2021.11.033

[28] C. J. Yao, W. G. Chen, L. Q. Li, K. Jiang, Z. G. Hu, J. M. Lin, N. Xu, J. Sun, J. D. Wu, Optics and Laser Technology 133, 106533 (2021); https://doi.org/10.1016/j.optlastec.2020.106533

[29] M. Amin, J. Tomko, J. J. Naddeo, R. Jimenez, D. M. Bubb, M. Steiner, J. Fitz-Gerald, S. M. O. Malley, 348, 30-37 (2015); https://doi.org/10.1016/j.apsusc.2014.12.191

[30] L. I. Ibarra-Rodriguez, J. C. Pantoja-Espinoza, E. Luevano-Hipolito, L. F. Garay-Rodríguez, A. Lopez-Ortiz, L. M. Torres-Martínez, V. H. Collins-Martínez, Journal of Photochemistry and Photobiology 11, 100125 (2022); https://doi.org/10.1016/j.jpap.2022.100125

[31] L. Liccardo, M. Bordin, P. M. Sheverdyaeva, M. Belli, P. Moras, A. Vomiero, E. Moretti, Advanced Functional Materials 33, 2212486 (2023); https://doi.org/10.1002/adfm.202212486

[32] P. Akhter, S. Nawaz, I. Shafiq, A. Nazir, S. Shafique, F. Jamil, Y. K. Park, M. Hussain, Molecular Catalysis 535, 112896 (2023); https://doi.org/10.1016/j.mcat.2022.112896

[33] N. Q. Luo, X. M. Tian, J. Xiao, W. Y. Hu, C. Yang, L. Li, D. H. Chen, Journal of Applied Physics 113, 164306 (2013); https://doi.org/10.1063/1.4803035